POLITECNICO DI TORINO
Repository ISTITUZIONALE

Improved antifouling and antibacterial properties of forward osmosis membranes through surface modification with zwitterions and silver-based metal organic frameworks

(Article begins on next page)

09 June 2026

Improved Antifouling and Antibacterial Properties of Forward Osmosis Membranes through Surface Modification with Zwitterions and Silver-based Metal Organic Frameworks

Mehdi Pejman,[a,1] Mostafa Dadashi Firouzjaei,[b,c,1] Sadegh Aghapour Aktij,[d, e] Parnab Das,[c] Ehsan Zolghadr,[f] Hesam Jafarian,[g] Ahmad Arabi Shamsabadi,[h] Mark Elliott,[e] Milad Rabbani Esfahani, [b,*] Marco Sangermano,[i] Mohtada Sadrzadeh,[d] Evan K. Wujcik,[b] Ahmad Rahimpour,[a,i, j,*] Alberto Tiraferri [a,*]

[a] Department of Environment, Land and Infrastructure Engineering (DIATI), Politecnico di Torino, Corso Duca degli Abruzzi 24, 10129 Turin, Italy

[b] Department of Chemical and Biological Engineering, University of Alabama, Tuscaloosa, AL, 35487, USA

[c] Department of Civil, Construction and Environmental Engineering, University of Alabama, Tuscaloosa 35487, USA

[d] Department of Chemical & Materials Engineering, University of Alberta, Edmonton, AB, T6G 1H9, Canada

[e] Department of Mechanical Engineering, 10-367 Donadeo Innovation Center for Engineering, Advanced Water Research Lab (AWRL), University of Alberta, Edmonton, AB, T6G 1H9, Canada

[f] Department of Physics and Astronomy, University of Alabama, Tuscaloosa, AL, 35487, USA

[g] Department of Mining and Metallurgical Engineering, Amirkabir University of Technology, Tehran, Iran

[h] Department of Chemistry, University of Pennsylvania, Philadelphia, Pennsylvania 19104, United States

[i] Department of Applied Science and Technology, Politecnico di Torino, Corso Duca Degli Abruzzi 24, 10129, Turin, Italy

[j] Department of Chemical Engineering, Babol Noushirvani University of Technology, Shariati Avenue, Babol Mazandaran, 4714871167, Iran

* Corresponding authors

[1] These authors contributed equally to this work

Abstract

This study investigates the effect of surface functionalization of a thin-film composite forward osmosis membrane with zwitterions and silver-based metal organic frameworks (Ag-MOFs) to improve the antifouling, anti-biofouling, and antimicrobial activity of the membrane. Two types of zwitterions, namely, 3-bromopropionic acid and 1,3-propane sultone, are chemically bonded, with and without incorporation of Ag-MOFs, over the surface of a polyamide membrane. Spectroscopy measurements indicate successful grafting of the modifying agents on the membrane surface. Contact angle measurements demonstrate a notable improvement in surface wettability upon functionalization. The performance of the membranes is evaluated in terms of water and salt fluxes in forward osmosis filtrations. The transport data show demonstrably increased water flux of around 300% compared to pristine membranes, with similar or slightly reduced salt reverse flux. The antifouling and anti-biofouling properties of the modified membranes are evaluated using sodium alginate and *E. coli*, respectively. These experiments reveal that functionalized membranes exhibit significant antifouling and anti-biofouling behavior, with high resilience against flux decline.

1. Introduction

The exponential growth of the world population represents a substantial pressure on our water resources. Increased water availability and better wastewater management may be promoted also through desalination and wastewater reuse [1]. Membrane-based technologies enable the extraction of high-quality water from various sources. Specifically, forward osmosis (FO) is an innovative process that makes use of thin-film composite (TFC) membranes and that has gained substantial academic and industrial interest in the past two decades. TFC FO membranes are high water permeability membranes with excellent salt rejection [2]. Fouling, however, remains the crippling technical challenge in FO, as well as in most membrane-based process. This phenomenon leads to a lowered water productivity and product quality, and it also reduces the useful timespan of the membrane while increasing the operational cost of the filtration process [3-5].

Bio-fouling, referred to as the "Achilles' heel" of membrane processes, occurs when microorganisms adhere onto the membrane surface and generate a new bio-layer, called biofilm [6]. The biofilm adds a resistance against mass transport, in addition to the hydraulic resistance of the membrane, thus necessitating the application of a larger driving force to maintain suitable productivity. Anchoring antimicrobial agents through surface modification of TFC membranes is another common strategy to tackle the biofouling issue through increasing the antimicrobial activity, surface hydrophilicity, and by reducing the surface roughness of the membrane [7, 8]. Several pathways have been adopted over the years to achieve these membrane features, including cross-linking [9, 10], in-situ covalent functionalization [11, 12], layer-by-layer assembly [9, 13], direct deposition of metal ions and nanoparticles [14, 15], and surface grafting [16, 17].

Previous studies have demonstrated the effectiveness of silver nanoparticles as biocides in membrane processes [18-20] due to their broad spectrum of antimicrobial activity, because silver particles are associated with both release-killing and contact-killing mechanisms [21]. In-situ surface functionalization of the commercial polyamide (PA) membranes with silver nanoparticles is a viable solution since it is cost-effective in terms of silver dosage compared to the direct injection of silver ions or particles into the feed solution. The in-situ approach minimizes the silver-induced health risks and bacterial resistance [22], and also allows for a relatively facile silver regeneration procedure [23]. Main issues of using silver particles for membrane modification remain the uncontrolled leaching of silver and the poor compatibility of these inorganic materials with the organic membrane matrix, possibly impairing the transport performance. In this respect, the use of metal organic frameworks (MOFs) is a promising option for a more rational use of silver.

MOFs consist of organic ligands connected by metal ions to form one-, two-, or three-dimensional coordination networks [24, 25]. Their key advantage over other structures is their tunability by using different metals and/or organic linkers. Also, their organic frame may ameliorate the interaction with the polyamide active layer of TFC membranes compared to other fully inorganic structures. MOFs tend to release metal ions, which then act as antimicrobial agents [26] and hence, silver-containing metal organic frameworks (Ag-MOFs) have been reported in such application by several researchers [27-29]. If antimicrobial activity should be paired with a better resistance to foulant adhesion, zwitterionic compounds are interesting materials for this purpose [30]. Zwitterions are overall neutral compounds with an equal number of positively and negatively charged functional groups. This architecture produces a strong binding property with water molecules, with the possibility to form a hydration layer [31]. For

this reason, several methods have been used to incorporate zwitterions at the membrane surface, including surface-initiated polymerization [32], grafting [33], and coating [34].

The hypothesis of this study is that zwitterions can be effectively combined with Ag-MOFs to impart different antifouling properties to the membrane surface. This functionalization may also improve the transport properties of FO membranes. Therefore, this study uses Ag-based MOFs combined with carboxyl (COO^-) and sulfur (SO_3^-)-containing zwitterions to develop novel antifouling/anti-biofouling TFC membranes via surface functionalization. The modifying agents are grafted on the surface of TFC FO membrane. The resulting membranes are thoroughly characterized to verify the success of the functionalization, and to analyze their new physio-chemical and morphological characteristics. The permeability and selectivity of the membranes are also evaluated in FO process. Finally, fouling and biofouling tests are performed to reveal the potential effect of the modifying agents.

2. Materials and Methods

2.1 Reagents

Silver nitrate ($AgNO_3$) as a source of metal, 2-methylimidazole (2MI) as an organic linker, and ethanol as a solvent were used for the synthesis of silver-based metal organic frameworks (Ag-MOFs). *N,N*-diethylethylenediamine (DEDA), potassium persulfate, and sodium metabisulfite were employed for the preparation of the grafting solutions. 3-bromopropionic acid (BPA) and 1,3-propane sultone (PS) were used as COO^--based and SO_3^--based zwitterions. For pH adjustment, nitric acid and sodium hydroxide were used. Sodium chloride (NaCl) was used for the preparation of the draw solution (DS) to perform the forward osmosis filtration tests. KCl

was used to prepare background solutions for streaming potential measurements. Deionized water (DI) was used for all purposes.

2.2 Preparation of Ag-MOFs

Ag-MOFs were prepared based on the optimization performed in a previous study [35]. Specifically, $AgNO_3$ (0.6 g) was dissolved in 90 mL of DI to prepare the metal solution, while the ligand solution was prepared by dissolving 1.05 g of 2MI in 90 of mL ethanol. The two solutions were stirred and then ultra-sonicated for 15 and 2 min, respectively. Then, the ligand solution was slowly poured into the metal solution followed by 30 min of stirring. The mixture was subsequently kept still for 3 h. The supernatant was carefully extracted using a syringe and discarded. The resulting suspension containing the precipitates was washed several times in order to remove the unreacted substances. Next, the precipitate was centrifuged twice with one round of rinsing with ethanol in each stage. Finally, the powder was collected and dried in an oven for 18 h at 60 °C.

2.3 Surface modification of membranes

The procedures adopted to obtain the functionalized membranes are the result of an initial experimental optimization, which is not reported below but briefly described in the Supporting Information. Specifically, the protocol to graft zwitterions on the surface of the commercial TFC membrane was adapted from a recent study by Yi *et al.* [36]. First, an aqueous solution containing DEDA (2% wt.), potassium persulfate (0.03% wt.), and sodium metabisulfite (0.02% wt.) at pH 5 was slowly poured on top of the membrane surface at room temperature for 60 min, which resulted in DEDA-grafted membrane via an amidation reaction between the carboxyl groups on the membrane surface and DEDA amine functional groups [37, 38].

The DEDA-grafted membrane was then covered by a PS aqueous solution (5% wt., pH 5.0) or a BPA solution (5% wt., pH 5.0), for 20 h at 40 °C, to graft SO_3^--based or COO^--based zwitterions, respectively. A mixture of NMP (10 wt.%) and water (90 wt.%) was used as a solvent to prepare the BPA solution to avoid agglomeration. These membranes are referred to as "PS zwitterionic (TFC-PS)" and "BPA zwitterionic (TFC-BPA)" TFC membranes. Functionalized membranes with Ag-MOFs were fabricated with the same procedure except that 0.05 wt.% of Ag-MOF was added to the to the PS aqueous solution (membrane referred to as "TFC-PS-MOF") and to the BPA solution (membrane referred to as "TFC-BPA-MOF"). Unmodified pristine membranes are hereafter referred to as "TFC0". The functionalization strategy is schematically presented in Scheme 1.
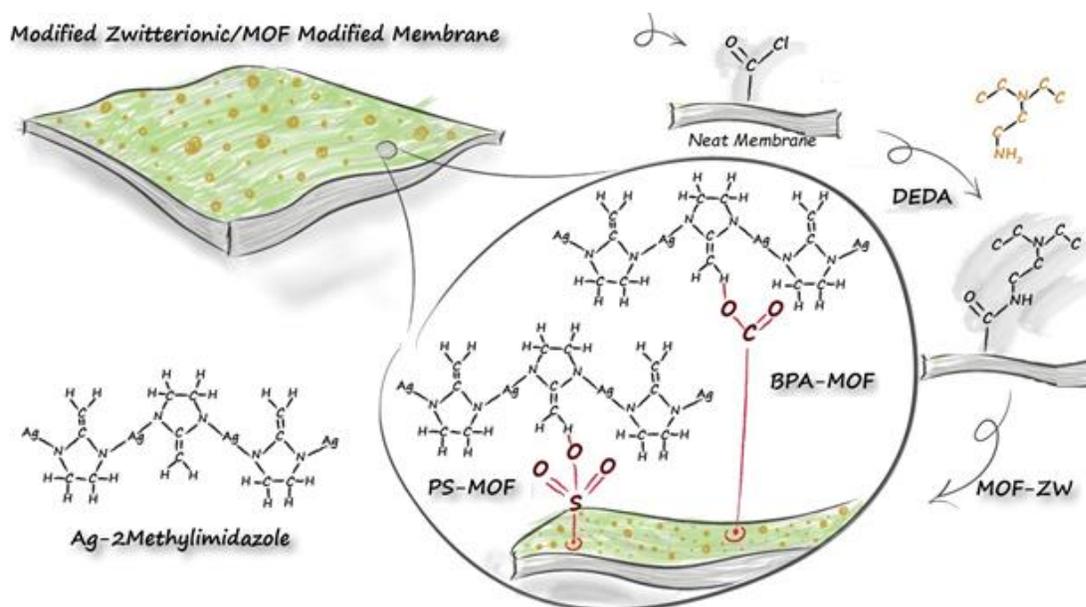
Scheme 1. Schematic illustration of the surface functionalization with zwitterions (BPA and PS) and Ag-MOF

2.4 Characterization of pristine and modified membranes

The chemical properties of the membrane surfaces were investigated by attenuated total reflection Fourier transform infrared spectroscopy (ATR-FTIR, Nicolet iS50 FT, Thermo Fisher Scientific, USA) in a scan range of 500–4000 cm^{-1}. Scanning electron microscopy (SEM, JEOL 7000, JEOL, USA) equipped with energy-dispersive X-ray spectroscopy (EDX, JEOL 7000, JEOL, USA) was used to characterize the top surface morphology of the membranes. The samples were coated with a 5-nm gold layer using a sputter coater (Leica EM ACE600, USA) before the measurements. Atomic force microscopy (AFM, EasyScan II, Switzerland) was used to investigate the topology and the roughness of the membrane surface, allowing the estimation of R_a (average roughness) and R_{RMS} (root-mean-squared roughness). Contact angle measurements (DSA 100, KRÜSS, Germany) of water droplets were performed on five random spots on the membrane samples to evaluate the degree of wettability of the membranes.

X-ray powder diffraction (XRD) spectra of the crystalline patterns corresponding to the fabricated MOF particles were obtained using a diffractometer (Bruker D8, Germany) with a Cu Kα radiation in 2θ mode from 0° to 60°. X-ray photoelectron spectroscopy (XPS) was performed with a Kratos spectrometer (Axis 165 XPS/ Auger, Shimadzu, Japan) equipped with a 100 μm monochromatic Al K(alpha) X-ray in order to identify the elemental composition and functional groups present on the surface of the membranes. The surface chemistry was further analyzed using Raman spectroscopy. Raman spectra were measured on a DXR Raman spectroscope (Thermo Scientific, U.S.A) equipped with a red excitation laser operating at 633 nm. Stokes Raman spectra were collected in the 100-2000 cm^{-1} range with a spectral resolution of 1.0 cm^{-1}. Zeta potential measurements were performed using a SurPASS Electrokinetic solid surface streaming potential analyzer (Anton Paar, Graz, Austria) to determine the surface potential of the

pristine and functionalized TFC membranes, across a 3-11 pH range. All the streaming potential measurements were conducted with the membrane immersed in a 1 mM KCl solution at 25 °C. HCl (0.05 M) and NaOH (0.05 M) were used for adjusting the pH of the KCl solution.

2.5 Assessment of transport parameters of the membranes

The transport parameters of the membranes, including the water permeance (A), the salt permeability coefficient (B), and the structural parameter of the support layer (S), were measured using a cross-flow FO unit with a cell containing a membrane with a net surface area of 30 cm^2. The system comprises two gear pumps circulating the draw solution (DS) and the feed solution (FS) on the two sides of the membrane at a cross-flow velocity of 20 cm/s. Deionized water and various NaCl solutions (concentrations of 0.5, 1, 1.5, and 2 M) were used as the FS and DS, respectively. The method proposed by Tiraferri et al. [39] was applied to determine the membranes transport parameters. Briefly, the methodology comprises a single FO experiment divided into four stages, each using a different concentration of DS. The experimental water and reverse salt fluxes measured in each stage are fitted to the corresponding FO transport equations by performing a least-squares non-linear regression, using A, B, and S as regression parameters.

2.6 Fouling and biofouling assessment procedure

Dynamic fouling experiments were carried out to evaluate the organic and bio-fouling propensity of the membranes, according to the procedure described in detail in previous studies [35]. In the case of organic fouling, sodium alginate (Sigma–Aldrich, St. Louis, MO), a polysaccharide, was selected as a model organic foulant [40-43]. A foulant solution was prepared by dissolving 250 mg/L of the sodium alginate powder in DI. The fouling experiments were conducted using initial feed and draw volumes of 3 L. Prior to the addition of the foulant, the permeate flux was allowed to stabilize at the value of 20 ± 1 L m^{-2}h^{-1} using the appropriate concentration of DS. The FO

9

system was then operated for 24 h (1440 min) at a cross-flow velocity of 8.5 cm/s, and the permeate flux was continuously monitored using an electronic balance. The flux of the clean membranes during the test was modeled to take into account the loss in flux due to mechanisms not related to fouling, i.e., the dilution of the draw solution and the reverse draw solute flux. For the biofouling assessment, *E. coli* bacteria at a concentration of about 10^7 CFU/L were added to the feed solution to accelerate biofouling following the same filtration procedure outlined above for the evaluation of organic fouling. The foulant concentrations during the tests represent conditions of accelerate fouling, being significantly higher than those encountered in typical operation [44, 45].

2.7 Anti-microbial activity of the functionalized membranes

The model gram-negative bacterium *Escherichia coli* (*E. coli*) was used to investigate the antimicrobial properties of the membranes. The *E. coli* bacteria were grown overnight in trypticase soy broth (TSB) with shaking and incubation at 37 °C. The fresh broth was then incubated with the overnight grown bacteria at 37 °C for 3 h. The number of attached live bacteria on the membrane surfaces was determined with two experimental procedures; confocal microscopy and heterotrophic plate count.

For the latter procedure, the bacterial culture was pelletized by centrifuging at 6000 rpm for 2 min and this bacterial stock was re-suspended in 1X sterile phosphate buffer saline (PBS) solution and a final concentration of 10^7 CFU/mL was achieved. For each membrane sample, a 2 cm^2 of membrane surface was placed in a sterile petri dish containing the bacterial solution and kept incubated at 37 °C with shaking for 1 h. The membranes were then washed three times in PBS solution to remove the unattached bacterial cells. The membranes were placed in a sterile plastic container with 10 mL of PBS solution and sonicated for 7 min to detach the bacteria. The

obtained solution was poured on TSB agar plates after appropriate dilutions and was incubated for 24 h at 37 °C. The number of viable bacterial cells on each plate was determined by counting the colony forming units (CFU) [35, 46].

In addition to the plate counting method, the viability of the bacteria upon contact with the membrane surface was determined using a LIVE/DEAD™ BacLight™ Bacterial Viability Kit (ThermoFisher Scientific). Specifically, SYTO 9 and propidium iodide (PI) stains were used to determine the number of viable and non-viable cells present on the surface of the membranes, respectively. A sample (1×1 cm^2) of each membrane was exposed to 1 mL of the bacterial solution and incubated for 1 h, and then the samples were washed in PBS solution to rinse away the unattached bacterial cells. The membranes were then stained with PI and SYTO9 stains and were incubated in a dark room for 15 min at room temperature. The membrane samples were washed with PBS solution to remove the excess stain prior to microscopy. The test membranes were mounted on a glass slide, covered with glass cover slip and examined under the confocal microscope [10, 47]. A Nikon C2 Laser Scanning Confocal Microscope was used for observing the number of dead and live *E. coli* cells. The laser for EGFP (Enhanced Green Fluorescent Protein) at 495-547 nm was used for the excitation of SYTO 9 and the laser for TRiC (T-complex protein-1 ring complex) at 566-624 nm was used for the excitation of PI stains. The live cells fluoresced green and the dead cells fluoresced red under the confocal microscope at a magnification of 60X lens at a scanning speed of one-half frame per second along with a digital image capture system. Eighteen images were taken at different spots for each bacterial membrane sample and the average of the counted cells was calculated for three sets of separate experiments. At least two sets of membrane samples were used to perform the bacteria contact experiment and the averages determined.

3. Results and Discussion

3.1 Successful functionalization and physio-chemical properties of the membrane surface
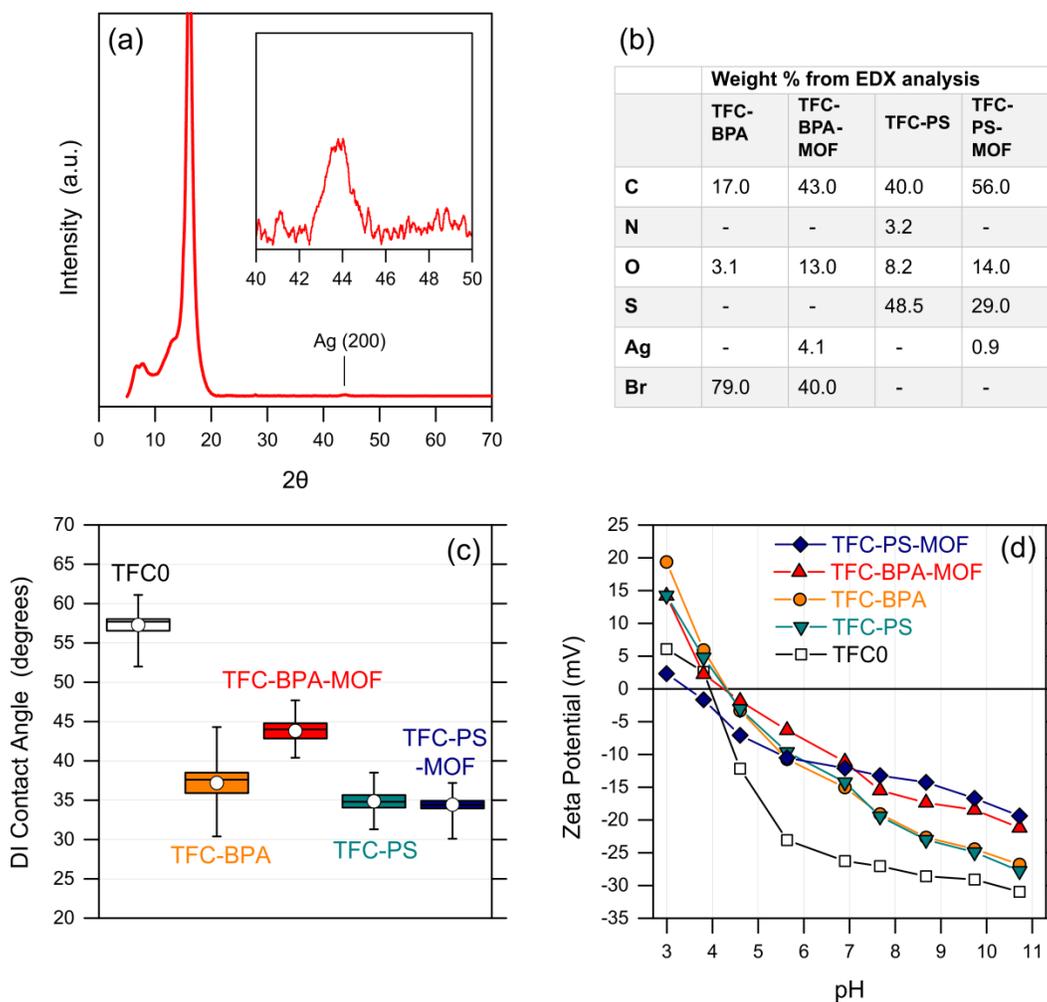
A series of surface characterizations was performed to assess the extent and the quality of the functionalization strategies. Infrared spectroscopy provides insight about the surface functional groups of unmodified and modified membranes (Figure 1a). The absorption peak at around 1620 cm^{-1} for all samples corresponds to the stretching vibration of C=O of the amide group, which is characteristic of PA membranes [48]. Peaks indicating the presence of zwitterions on the surface of modified membranes were observed at wavenumbers 1030 cm^{-1} and 1730 cm^{-1}, which are assigned to the presence of the O=S=O functional group of PS and the C=O functional group of BPA, respectively, thus suggesting the successful grafting of zwitterions on the surface of TFC FO membranes. This result is in accordance with previous studies [36]. Raman spectroscopy was also employed to corroborate the results from infrared spectroscopy and the spectra for TFC0, TFC-BPA, TFC-BPA-MOF, TFC-PS, and TFC-PS-MOF samples are presented in Figure 1b. The dominant peak at 940 cm^{-1} observed for all the samples is related to several modes of polyamide, corresponding mostly to C-C deformation, C-O-C stretching, and C-C=O. Moreover, the band at 1188 cm^{-1} is ascribed to the superposition of C-N stretching and C-N-H wagging in the amide. The peak centered at 1281 cm^{-1} is instead associated with CH_2 deformations and NH_2 bending modes in the amide [49]. The peaks around 980 cm^{-1}, 1010 cm^{-1}, and 1065 cm^{-1} are attributed to the symmetric stretching modes of SO_3 [50-53]. These SO_3 Raman marker bands are another proof of the presence of PS zwitterion, specifically on TFC-PS membranes. These peaks were less prominent on TFC-PS-MOF compared to TFC-PS, possibly due to the presence of Ag-MOFs, which may lead to different Raman modes. In addition, the peak around 1127 cm^{-1} observed for TFC-PS and TFC-PS-MOF membranes is also assigned to an asymmetric stretching

mode of SO_3 [53], further corroborating the successful grafting of PS zwitterion on the surface of TFC-PS and TFC-PS-MOF membranes. On the other hand, the peak around 410 cm^{-1} in the spectrum of TFC-BPA-MOF sample is correlated to C-Br bonding, and specifically to its stretching mode, which points to the presence of BPA on the surface; the extra peak centered at 825 cm^{-1} is also attributable to C-Br bonding [49] and most probably caused by stretching vibration [54]. One would also expect peaks in the range of 100-150 cm^{-1} corresponding to the Ag-Ag bonding for TFC-BPA-MOF and TFC-PS-MOF samples; however, these peaks were not observed, probably due to the small values of Raman shift. These peaks are most likely covered by the exciting laser light shoulder. However, the presence of Ag can be demonstrated through XRD and XPS investigation.
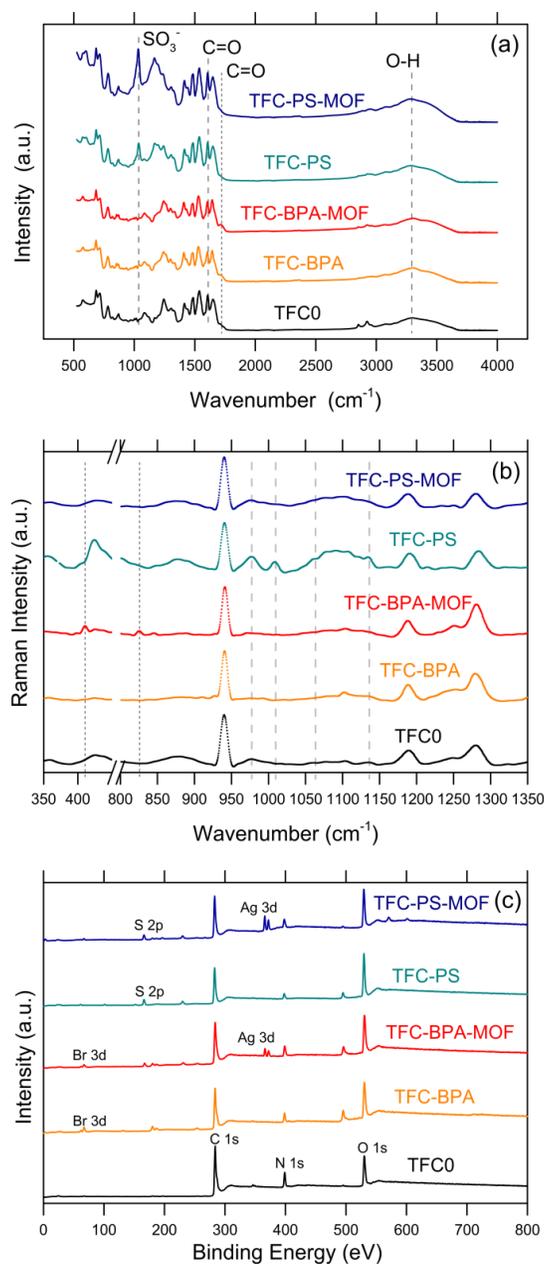
Figure 1. Physio-chemical characteristics of the surface of the membranes: (a) ATR-FTIR spectra: peaks indicating the successful implementation of zwitterions are highlighted; (b) Raman spectra: short dash and long dash lines indicates the Raman shift associated with SO_3 and C-Br modes, respectively; (c) XPS survey spectra: the corresponding peaks for C 1s, N 1s, O 1s, Br 3d, S 2p, and Ag 3d are marked. Please note that XPS peaks at 495 eV and ~1070 eV (not shown) are associated with the Auger line of Na KLL and with Na 1s peak [55-58], respectively, possibly due to some contamination.

Indeed, XRD analysis shows Ag (200) characteristic peaks on both TFC-BPA-MOF and TFC-PS-MOF membranes, as presented in Figure 2a and in Figure S1 of the Supporting Information. The weakness of these peaks can be attributed to the low concentration of Ag-MOFs present on the surface of the membranes. Much further insight into the surface elemental composition was obtained with X-ray photoelectron spectroscopy. The XPS survey spectra are presented in Figure 1c and show three dominant peaks around 284, 399, and 530 eV for all the samples. These bands correspond to the predominant elements of carbon (C 1s), nitrogen (N 1s), and oxygen (O 1s), respectively [59, 60]. The deconvoluted C 1s, O 1s, Br 3d, S 2p, and Ag 3d high-resolution XPS spectra are shown in Figure S2 of the Supporting Information, where all fitted peaks are plotted using Gaussian functions. A detailed discussion about the different spectra and peaks accompany them in the Supporting Information. Briefly, the peaks related to C 1s and O 1s are characteristics of polyamide [61-65]. For TFC-BPA and TFC-BPA-MOF, the Br bonds centered at 67 eV are an indication of the successful grafting of BPA zwitterions on the membrane surfaces [66, 67]. On the other hand, the S bonds around 166 eV for TFC-PS and TFC-PS-MOF suggest the successful grafting of PS zwitterions [62, 68, 69]. Finally, the appearance of Ag-related peaks for TFC-BPA-MOF and TFC-PS-MOF around 366 eV and 372 eV reveals the presence of Ag-MOFs on the surface of these two membranes [70, 71]. The grafting of zwitterions and the presence of silver on the surface structure of functionalized membranes are further corroborated qualitatively by EDX results, summarized in Figure 2b and obtained from the survey results reported in Figure S3 of the Supporting Information.

	Weight % from EDX analysis			
	TFC-BPA	TFC-BPA-MOF	TFC-PS	TFC-PS-MOF
C	17.0	43.0	40.0	56.0
N	-	-	3.2	-
O	3.1	13.0	8.2	14.0
S	-	-	48.5	29.0
Ag	-	4.1	-	0.9
Br	79.0	40.0	-	-

Figure 2. Physio-chemical characteristics of the surface of the membranes: (a) XRD spectrum of TFC-BPA-MOF, chosen as a representative membrane, with inset graph highlighting the peak related to Ag(200); (b) EDX analysis in terms of weight percentage of the various elements; (c) statistics of contact angles of DI water droplets sitting on the membrane surface; (d) zeta potential measured as a function of pH, measured in a 1 mM KCl solution.

The spectroscopic analyses presented so far strongly indicate the suitable functionalization of the surfaces with the desired modifying agents, specifically, the two different zwitterions and the additional availability of Ag-MOFs for two of the membranes. Further information on the characteristics of the functionalized surfaces can be obtained with respect to surface charge and wettability. These parameters are indirectly related once again to the extent of functionalization, but they have a rather more interestingly effect on the transport and fouling behavior of the membranes. The surface zeta potentials were measured over the pH range of 3 to 11 and the results are plotted in Figure 2d. The pristine sample (TFC0) exhibited a negative potential for pH values above the pK_a of carboxyl groups [72]. The presence of overall electrically neutral zwitterions led to a shift towards less negative zeta potential values. This effect was even more pronounced following modification with Ag-MOFs for the TFC-BPA-MOF and TFC-PS-MOF membranes, possibly due to the addition of positively charged silver within the Ag-MOF structure. Maintaining an overall negative potential at near neutral pH while minimizing the exposed density of carboxyl groups is a valid strategy to exploit the electrostatic repulsion toward organic and biological foulants while minimizing the possibility of carboxyl interaction with calcium and other multivalent cations, which has been shown to promote the formation of densely packed fouling layers [73, 74]. The wettability of the surfaces, another property strongly associated with antifouling behavior, was estimated with water contact angle measurements. The results (Figure 2c) show a decline from roughly 57° for the pristine TFC0 membrane to approximately 37°, 44°, 35°, and 34° for TFC-BPA, TFC-BPA-MOF, TFC-PS, and TFC-PS-MOF, respectively. This observation may be rationalized with the presence of zwitterions, which lead to an increased affinity between the membrane surface and water droplets.

17

3.2 Morphological properties of the membrane surface

Another parameter influencing the deposition of foulants onto the membrane is surface morphology, often described in terms of roughness. The surface morphology of the membranes is shown in Figure 3. The representative SEM micrograph of the pristine membrane (Figure 3a) shows the typical leaf-like or ridge-and-valley structure of PA membranes prepared by interfacial polymerization of MPD and TMC [73, 75]. These ridge-and-valley structures were slightly altered following grafting of zwitterions, and more markedly after the incorporation of Ag-MOFs (Figure 3b-e). Specifically, by observing the SEM micrographs related to TFC-BPA-MOF and TFC-PS-MOF, nodules were observed in the presence of Ag-MOFs. Atomic force microscopy results were in accordance with SEM measurements. AFM roughness scans and the extracted parameters, R_a (average roughness) and R_{RMS} (root-mean-squared roughness), are presented in Figure S4 of the Supporting Information and in Figure 3a of the main manuscript, respectively. The membrane surface roughness generally increased as a result of functionalization. This change was smaller when only zwitterions were used for surface modification, while more increment in roughness was observed when Ag-MOFs were also incorporated, possibly associated with the nodules observed from SEM analysis. Normally, larger roughness is associated with increased fouling propensity and our observations underline a typical trade-off of membrane surface functionalization approaches. However, the Wenzel model of wetting suggests that surface roughness may amplify the wettability behavior of the original surface; hence, wettable surfaces may become more wettable, and vice versa. Therefore, one might argue that the synergetic effect of a reduced contact angle and increased roughness can ultimately lead to a more wettable surface for the membranes modified with Ag-MOFs [76].
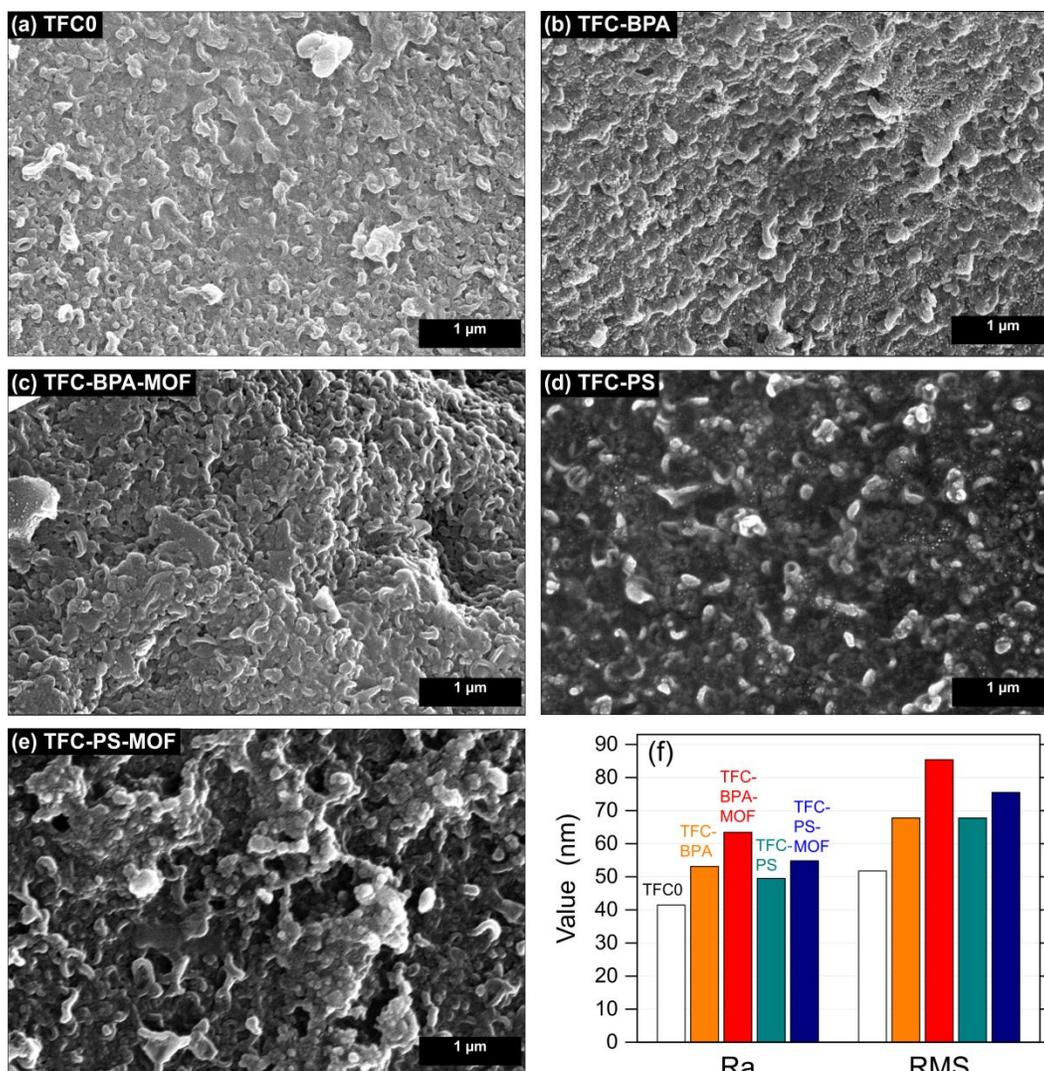
Figure 3. (a-e) Representative SEM micrographs and (f) rougness parameters of the pristine and functionalized membranes.

3.3 The membranes showed high performance in forward osmosis

Most membrane functionalization studies show that the transport behavior of the membranes change upon modification, often resulting in membranes with reduced performance. Filtration experiments were thus performed to assess the suitability of the surface-functionalized membranes for the specific FO process targeted in this study. Figure 4 illustrates the water flux

(J_w) and reverse solute flux (J_s) values determined at different DS concentrations. Interestingly, the water flux of membranes exposing PS zwitterions was considerably higher than the water flux of both pristine and BPA zwitterion-functionalized membranes. In fact, the membranes modified with PS, with and without Ag-MOFs, exhibited the highest productivity, while those functionalized with BPA zwitterions were associated with the lowest value of water flux. One may expect that the presence of zwitterions would increase the water permeability through a better ability to interact with water molecules; on the other hand, BPA zwitterions may have produced a dense layer which overall increased the resistance against water permeation. This rationalization may be also supported by the SEM micrographs in Figure 3b, c. In general, the interaction between Ag^+ and the functional groups of zwitterions (COO^- and SO_3^-) seemed to lead to the formation of a more favorable structure for water permeation, as TFC-BPA-MOF and TFC-PS-MOF membranes exhibited fluxes that were higher than those measured with TFC-BPA and TFC-PS membranes, respectively.
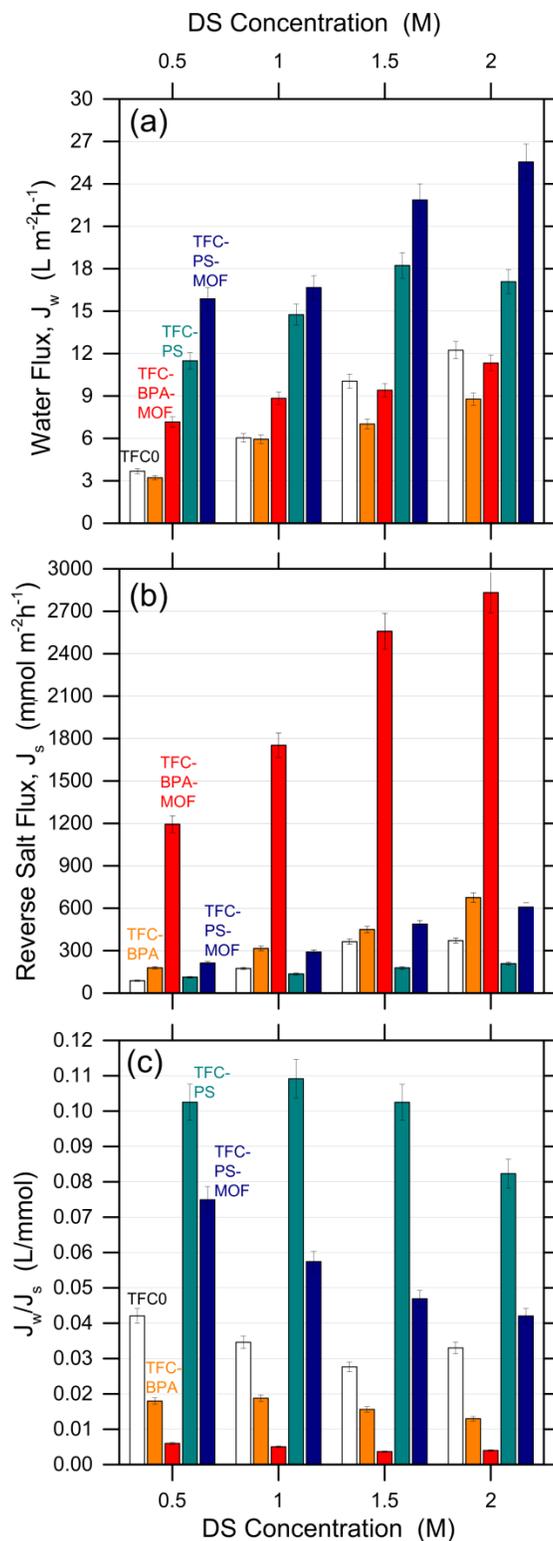
Figure 4. Performance of the pristine TFC and functionalized membranes in FO filtration tests at various DS concentrations: a) FO water flux, J_w, b) FO reverse salt flux, J_s, c) water flux to salt flux ratio, J_w/J_s.

The reverse solute flux of membranes functionalized with zwitterions and Ag-MOFs- zwitterions increased compared to the pristine membrane, with the exception of TFC-PS, which showed no considerable change. The increment in solute flux permeability may be partly explained by the reduced negative charge of the membrane surface after functionalization with zwitterions and Ag-MOFs. This result can reduce the electrostatic repulsion at the membrane active layer/feed solution interface, leading to a higher solute permeability (B) and hence, a higher reverse solute flux. The considerable increase of reverse solute flux in the case of TFC-BPA-MOF may be specifically attributed to the addition of BPA-based Ag-MOFs to the membrane surface, which can lead to change in charge distribution [77]. The Jw/Js ratio, or reverse solute flux selectivity, is an important parameter including the effect on both membrane productivity and selectivity, and defined as the volume of water produced per mass of draw solute lost due to back diffusion [78-80]. Higher values are indicative of membranes with improved transport performance [81]. As illustrated in Figure 4c, TFC-PS and TFC-PS-MOF membranes displayed a significant improvement in terms of Jw/Js values in comparison with the TFC0 pristine membrane, while TFC-BPA and TFC-BPA-MOF samples performed poorly in that regard. Conclusions that can be drawn based on the FO performance results is therefore that BPA zwitterions might not be able to enhance the membrane transport parameters as favorably as PS zwitterions, and that the addition of Ag-MOFs promoted productivity at the expense of some selectivity.

3.4 The membranes comprising silver-based MOF showed considerable antibacterial activity

Both plate count and confocal microscopy were used to determine the antimicrobial characteristics of the membranes, using *E. coli* as a surrogate for biofouling organisms. Figure 5 includes a pictorial representation of the live and dead bacterial cells as observed under the

22

confocal microscope and the bacterial colonies grown on the TSB agar plates. Using the culture-based pour plating method, the TFC-BPA-MOF membrane yielded approximately 100% (>99.999%) die-off of *E. coli* relative to a solution of 10^7 *E. coli* CFU/mL. The TFC-PS-MOF membrane yielded a substantial 62% die-off of *E. coli*. The TFC-BPA and TFC-PS membranes (those without Ag-MOFs) yielded small reductions of 10% and 14%, respectively, while the TFC0 membrane yielded an *E. coli* reduction of 5%, implying a lack of antibacterial properties. To further investigate the bactericidal activities of the functionalized membranes, fluorescence images were taken with the confocal microscope after exposing the membrane to *E. coli* and staining with SYTO9 and PI, the standard stains used to differentiate viable and non-viable cells. The live (green):dead (red) ratio was used to describe the relative viability of the bacterial cells on the membrane surface. The ratio of living-to-dead cells was very high (approximately 100) for the TFC0 membrane, i.e., 100 live *E. coli* bacteria for every dead bacterium. In contrast, the ratio for the TFC-BPA-MOF membrane was 0.01, meaning only one living bacterium for every 100 dead bacteria, and indicating approximately 99% die-off of the attached bacteria. The TFC-PS-MOF membrane had a live-to-dead ratio of 0.33, indicating three dead bacteria for every living bacterium (75% die-off), whereas TFC-BPA and TFC-PS (with zwitterions but without Ag-MOFs) yielded ratios of 6.66 (13% die-off) and 5.22 (16% die-off), respectively. The analysis of the bacterial solution showed all green (living) bacterial cells, confirming the viability of the model bacteria.
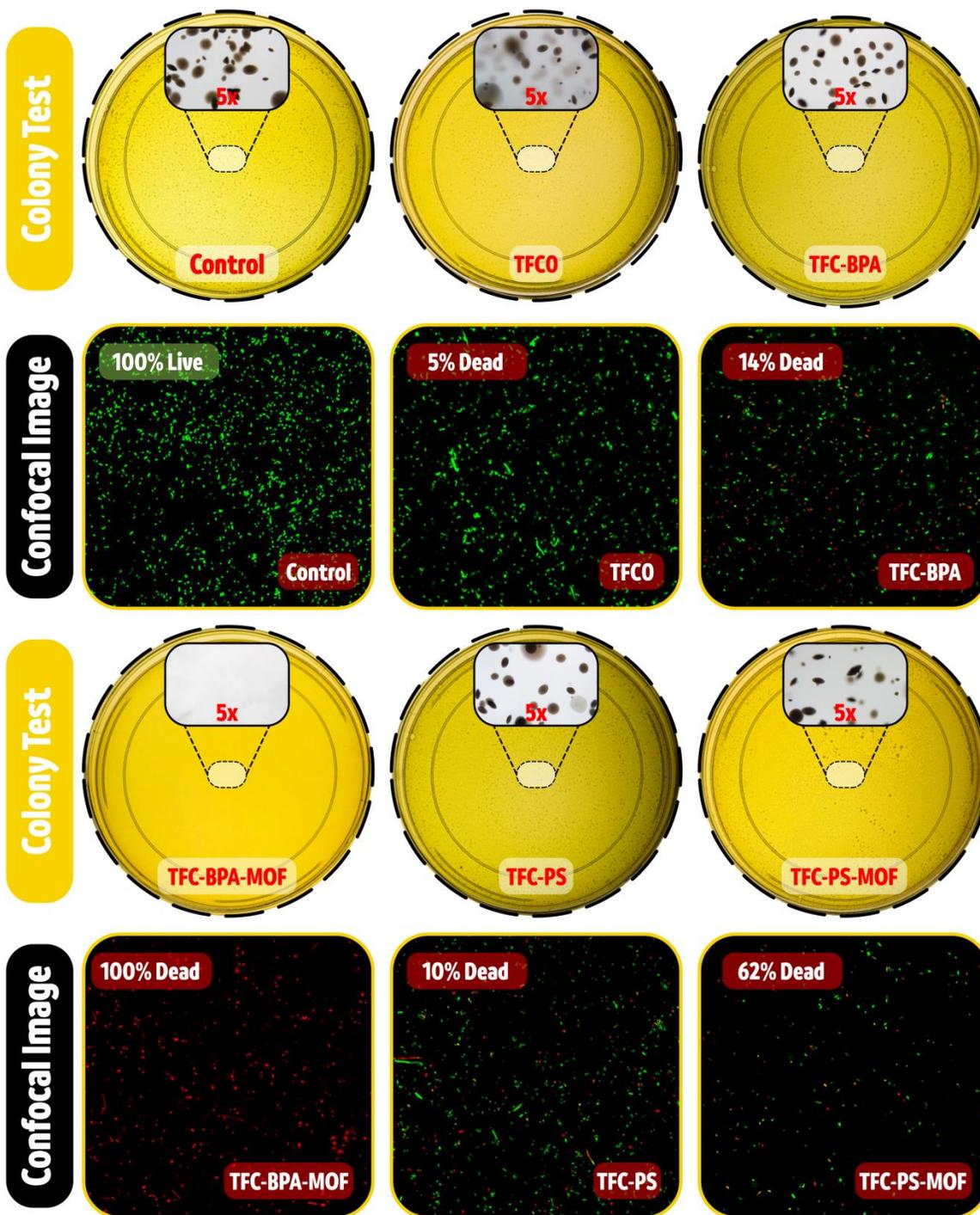
Figure 5. Results of antimicrobial activity tests for pristine and functionalized membranes tested with gram-negative *E. coli* using heterotrophic plate count and confocal microscopy.

The two methods of assessing antimicrobial activity, culture-based and confocal fluorescence microscopy, yielded similar results. In both cases, the TFC-BPA-MOF membrane, functionalized with the zwitterion BPA and Ag-MOFs, achieved the best performance, with nearly complete (99% or greater) inactivation of *E. coli* bacteria, while the TFC-PS-MOF membrane yielded substantial (62-75%) inactivation but far less than that observed for TFC-BPA-MOF. In both assays, the membranes functionalized with zwitterions only (TFC-BPA and TFC-PS) showed little inactivation of *E. coli* (10-16%) and the pristine TFC0 membrane showed almost no antimicrobial activity with only 1-5% die-off. The antibacterial property of TFC-BPA-MOF and TFC-PS-MOF membranes is imparted by the Ag-MOFs available at their surface. During application, Ag-MOFs would be a reservoir of silver ion (Ag^+) that would create sustainable antibacterial activity [82]. Moreover, the 2-metylimidazol organic linkers applied in this study to synthesize the Ag-MOFs itself had antimicrobial activity and therefore a synergetic effect may be attained [83].

3.5 The flux reduction due to fouling was alleviated

Fouling tests were conducted using sodium alginate (SA) as model organic foulant and *E. coli* as model biofoulant. SA is a polysaccharide and one of the main components of extracellular polymeric substances. During the tests, the water flux started to decrease substantially soon after the introduction of SA into the FS (Figure 6a). This decrease was observed for all the membranes; however, the functionalized membranes demonstrated a relatively lower flux decline. This result can be justified by the fact that the functionalized membranes possessed a more hydrophilic surface that gave rise to a denser hydration layer, which hampered foulant deposition on the membrane surface [84]. The presence of Ag-MOFs on the TFC-BPA-MOF and TFC-PS-MOF membranes also seemed to lead to a relative improvement in antifouling

25

propensity compared to membranes solely modified by zwitterions. A possible explanation is that the presence of 2-methylimidazol in the structure of Ag-MOFs might help forming an even stronger hydration layer on the membrane surface [85]. The results of biofouling experiments are presented in Figure 6b. As expected, introducing *E. coli* into the feed solution caused the water flux to decrease in time due to deposition and possible biofilm formation on the membrane surface. This phenomenon was somewhat thwarted in the case of functionalized membranes, and this positive effect was generally more pronounced in the case of TFC-BPA-MOF and TFC-PS-MOF with respect to TFC-BPA and TFC-PS samples. This result can be attributed to the presence of silver-containing MOFs with anti-microbial activity.
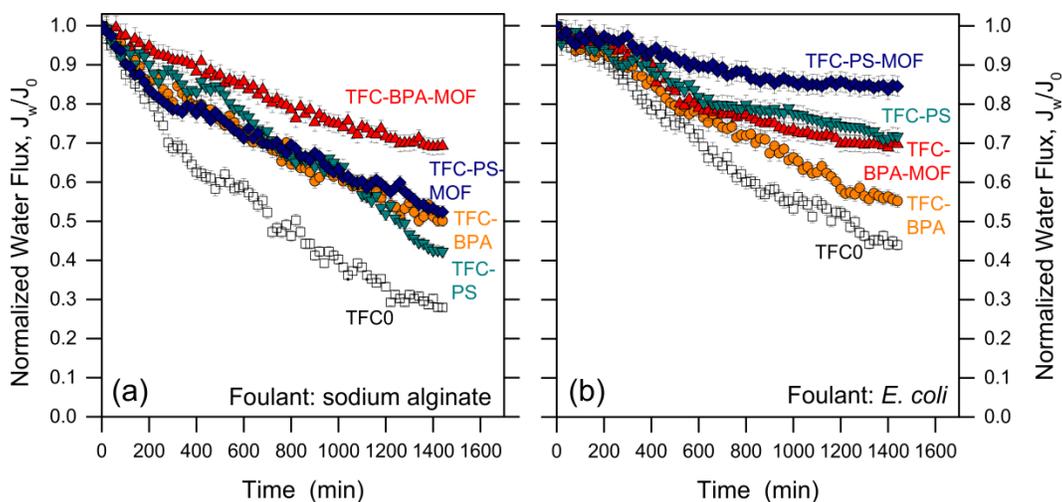
Figure 6. Flux decline due to fouling in FO experiments for the pristine and the surface-modified membranes; a) organic fouling by sodium alginate at a concentration of 250 mg/L, b) microbial biofouling by *E. coli* with an initial concentration of 10^7 CFU/L.

4. Conclusions

Ag-MOFs, together with COO^-- and SO_3^--based zwitterions were used to functionalize the surface of TFC FO membranes to develop their antifouling properties. The characterization of

26

the functionalized membranes revealed the availability of Ag-MOFs and zwitterions, and a more wettable surface for the membranes upon functionalization. The water productivity and the solute selectivity in FO were mostly maintained or in some cases were improved compared to the pristine membranes. Specifically, the membranes functionalized with 1,3-propane sultone (PS) exhibited a highly enhanced water flux while maintaining a low reverse salt flux. On the other hand, while BPA-functionalized membranes showed a slightly reduced transport performance, they demonstrated a higher anti-bacterial capability. Assays for culturable bacteria suggested a significant fraction of dead cells upon contact with the functionalized membranes comprising silver-based MOFs, namely 100% for TFC-BPA-MOF and 62% for TFC-PS-MOF, respectively. In FO filtration tests, these results translated into a lower tendency for flux reduction compared to the pristine membrane in the presence of sodium alginate or *E. coli*. In regard to the objectives of this study, the membrane functionalized with PS and Ag-MOFs (TFC-PS-MOF) was the best candidate amongst the four because of the combination of highest anti-biofouling capacity, highest FO flux, substantial rate of biocidal activity, and enhanced perm-selectivity compared to the pristine membrane. In summary, the surface functionalization with Ag-MOFs and PS zwitterions is a promising option to enhance the anti-fouling properties of TFC FO membranes.

Declaration of competing interest

The authors declare no competing financial interest.

Acknowledgments

Appendix A. Supporting Information. Information on experimental optimization to attain the final membrane functionalization protocols; XRD spectrum of membrane TFC-PS-MOF; Additional details about XPS results; EDX spectra; Representative AFM 3D images of the membrane surfaces.

References

[1] N. Akther, A. Sodiq, A. Giwa, S. Daer, H.A. Arafat, S.W. Hasan, Recent advancements in forward osmosis desalination: A review, Chem. Eng. J., 281 (2015) 502-522. https://doi.org/10.1016/J.CEJ.2015.05.080

[2] N.Y. Yip, A. Tiraferri, W.A. Phillip, J.D. Schiffman, M. Elimelech, High Performance Thin-Film Composite Forward Osmosis Membrane, Environ. Sci. Technol., 44 (2010) 3812-3818. https://doi.org/10.1021/es1002555

[3] A.W. Mohammad, C.Y. Ng, Y.P. Lim, G.H. Ng, Ultrafiltration in Food Processing Industry: Review on Application, Membrane Fouling, and Fouling Control, Food Bioprocess Technol., 5 (2012) 1143-1156. https://doi.org/10.1007/s11947-012-0806-9

[4] M.D. Firouzjaei, S.F. Seyedpour, S.A. Aktij, M. Giagnorio, N. Bazrafshan, A. Mollahosseini, F. Samadi, S. Ahmadalipour, F.D. Firouzjaei, M.R. Esfahani, A. Tiraferri, M. Elliott, M. Sangermano, A. Abdelrasoul, J.R. McCutcheon, M. Sadrzadeh, A.R. Esfahani, A. Rahimpour, Recent advances in functionalized polymer membranes for biofouling control and mitigation in forward osmosis, (2019) 117604-117604. https://doi.org/10.1016/j.memsci.2019.117604

[5] Q. She, R. Wang, A.G. Fane, C.Y. Tang, Membrane fouling in osmotically driven membrane processes: A review, J. Membr. Sci., 499 (2016) 201-233. https://doi.org/10.1016/j.memsci.2015.10.040

[6] H.C. Flemming, G. Schaule, T. Griebe, J. Schmitt, A. Tamachkiarowa, Biofouling—the Achilles heel of membrane processes, Desalination, 113 (1997) 215-225. https://doi.org/10.1016/S0011-9164(97)00132-X

[7] J. Zhu, A. Uliana, J. Wang, S. Yuan, J. Li, M. Tian, K. Simoens, A. Volodin, J. Lin, K. Bernaerts, Y. Zhang, B. Van der Bruggen, Elevated salt transport of antimicrobial loose nanofiltration membranes enabled by copper nanoparticles via fast bioinspired deposition, J. Mater. Chem. A, 4 (2016) 13211-13222. https://doi.org/10.1039/C6TA05661J

[8] N. Misdan, W.J. Lau, A.F. Ismail, Seawater Reverse Osmosis (SWRO) desalination by thin-film composite membrane—Current development, challenges and future prospects, Desalination, 287 (2012) 228-237. https://doi.org/10.1016/J.DESAL.2011.11.001

[9] Q. Chen, P. Yu, W. Huang, S. Yu, M. Liu, C. Gao, High-flux composite hollow fiber nanofiltration membranes fabricated through layer-by-layer deposition of oppositely charged crosslinked polyelectrolytes for dye removal, J. Membr. Sci., 492 (2015) 312-321. https://doi.org/10.1016/J.MEMSCI.2015.05.068

[10] A. Rahimpour, S.F. Seyedpour, S. Aghapour Aktij, M. Dadashi Firouzjaei, A. Zirehpour, A. Arabi Shamsabadi, S. Khoshhal Salestan, M. Jabbari, M. Soroush, Simultaneous Improvement of Antimicrobial, Antifouling, and Transport Properties of Forward Osmosis Membranes with Immobilized Highly-Compatible Polyrhodanine Nanoparticles, Environ. Sci. Technol., 52 (2018) 5246-5258. https://doi.org/10.1021/acs.est.8b00804

[11] M. Di Vincenzo, M. Barboiu, A. Tiraferri, Y.M. Legrand, Polyol-functionalized thin-film composite membranes with improved transport properties and boron removal in reverse osmosis, J. Membr. Sci., 540 (2017) 71-77. https://doi.org/10.1016/J.MEMSCI.2017.06.034

[12] L. Yang, Z. Wang, J. Zhang, Highly permeable zeolite imidazolate framework composite membranes fabricated via a chelation-assisted interfacial reaction, J. Mater. Chem. A, 5 (2017) 15342-15355.

https://doi.org/10.1039/C7TA03244G

[13] Y.-H. La, J. Diep, R. Al-Rasheed, D. Miller, L. Krupp, G.M. Geise, A. Vora, B. Davis, M. Nassar, B.D. Freeman, M. McNeil, G. Dubois, Enhanced desalination performance of polyamide bi-layer membranes prepared by sequential interfacial polymerization, J. Membr. Sci., 437 (2013) 33-39. https://doi.org/10.1016/J.MEMSCI.2013.02.044

[14] M. Ben-Sasson, K.R. Zodrow, Q. Genggeng, Y. Kang, E.P. Giannelis, M. Elimelech, Surface Functionalization of Thin-Film Composite Membranes with Copper Nanoparticles for Antimicrobial Surface Properties, Environ. Sci. Technol., 48 (2014) 384-393. https://doi.org/10.1021/es404232s

[15] Z. Yang, Y. Wu, J. Wang, B. Cao, C.Y. Tang, *In Situ* Reduction of Silver by Polydopamine: A Novel Antimicrobial Modification of a Thin-Film Composite Polyamide Membrane, Environ. Sci. Technol., 50 (2016) 9543-9550. https://doi.org/10.1021/acs.est.6b01867

[16] W. Ding, J. Cai, Z. Yu, Q. Wang, Z. Xu, Z. Wang, C. Gao, Fabrication of an aquaporin-based forward osmosis membrane through covalent bonding of a lipid bilayer to a microporous support, J. Mater. Chem. A, 3 (2015) 20118-20126. https://doi.org/10.1039/C5TA05751E

[17] H.M. Hegab, A. ElMekawy, T.G. Barclay, A. Michelmore, L. Zou, C.P. Saint, M. Ginic-Markovic, Fine-Tuning the Surface of Forward Osmosis Membranes via Grafting Graphene Oxide: Performance Patterns and Biofouling Propensity, ACS Appl. Mater. Interfaces, 7 (2015) 18004-18016. https://doi.org/10.1021/acsami.5b04818

[18] A. Dror-Ehre, A. Adin, G. Markovich, H. Mamane, Control of biofilm formation in water using molecularly capped silver nanoparticles, Water Res., 44 (2010) 2601-2609. https://doi.org/10.1016/J.WATRES.2010.01.016

[19] Y. Liu, E. Rosenfield, M. Hu, B. Mi, Direct observation of bacterial deposition on and detachment from nanocomposite membranes embedded with silver nanoparticles, Water Res., 47 (2013) 2949-2958. https://doi.org/10.1016/J.WATRES.2013.03.005

[20] M.S. Mauter, Y. Wang, K.C. Okemgbo, C.O. Osuji, E.P. Giannelis, M. Elimelech, Antifouling Ultrafiltration Membranes via Post-Fabrication Grafting of Biocidal Nanomaterials, ACS Appl. Mater. Interfaces, 3 (2011) 2861-2868. https://doi.org/10.1021/am200522v

[21] Z. Li, D. Lee, X. Sheng, R.E. Cohen, M.F. Rubner, Two-Level Antibacterial Coating with Both Release-Killing and Contact-Killing Capabilities, Langmuir, 22 (2006) 9820-9823. https://doi.org/10.1021/la0622166

[22] D. Roy, T.E. Furtak, Evidence for Ag cluster vibrations in enhanced Raman scattering from the Ag/electrolyte interface, Chem. Phys. Lett., 124 (1986) 299-303. https://doi.org/10.1016/0009-2614(86)85021-7

[23] M. Ben-Sasson, X. Lu, E. Bar-Zeev, K.R. Zodrow, S. Nejati, G. Qi, E.P. Giannelis, M. Elimelech, In situ formation of silver nanoparticles on thin-film composite reverse osmosis membranes for biofouling mitigation, Water Res., 62 (2014) 260-270. https://doi.org/10.1016/J.WATRES.2014.05.049

[24] S. Kitagawa, R. Kitaura, S.-i. Noro, Functional Porous Coordination Polymers, Angew. Chem., Int. Ed., 43 (2004) 2334-2375. https://doi.org/10.1002/anie.200300610

[25] N. Yin, K. Wang, L. Wang, Z. Li, Amino-functionalized MOFs combining ceramic membrane ultrafiltration for Pb (II) removal, Chem. Eng. J., 306 (2016) 619-628. https://doi.org/10.1016/J.CEJ.2016.07.064

[26] J. Quirós, K. Boltes, S. Aguado, R.G. de Villoria, J.J. Vilatela, R. Rosal, Antimicrobial metal–organic

frameworks incorporated into electrospun fibers, Chem. Eng. J., 262 (2015) 189-197. https://doi.org/10.1016/J.CEJ.2014.09.104

[27] X. Lu, J. Ye, D. Zhang, R. Xie, R.F. Bogale, Y. Sun, L. Zhao, Q. Zhao, G. Ning, Silver carboxylate metal–organic frameworks with highly antibacterial activity and biocompatibility, J. Inorg. Biochem., 138 (2014) 114-121. https://doi.org/10.1016/J.JINORGBIO.2014.05.005

[28] K. Martín-Betancor, S. Aguado, I. Rodea-Palomares, M. Tamayo-Belda, F. Leganés, R. Rosal, F. Fernández-Piñas, Co, Zn and Ag-MOFs evaluation as biocidal materials towards photosynthetic organisms, Sci. Total Environ., 595 (2017) 547-555. https://doi.org/10.1016/j.scitotenv.2017.03.250

[29] M. Berchel, T.L. Gall, C. Denis, S.L. Hir, F. Quentel, C. Elléouet, T. Montier, J.-M. Rueff, J.-Y. Salaün, J.-P. Haelters, G.B. Hix, P. Lehn, P.-A. Jaffrès, A silver-based metal–organic framework material as a 'reservoir' of bactericidal metal ions, New J. Chem., 35 (2011) 1000-1000. https://doi.org/10.1039/c1nj20202b

[30] J. Meng, Z. Cao, L. Ni, Y. Zhang, X. Wang, X. Zhang, E. Liu, A novel salt-responsive TFC RO membrane having superior antifouling and easy-cleaning properties, J. Membr. Sci., 461 (2014) 123-129. https://doi.org/10.1016/j.memsci.2014.03.017

[31] P. Kaner, E. Rubakh, D.H. Kim, A. Asatekin, Zwitterion-containing polymer additives for fouling resistant ultrafiltration membranes, J. Membr. Sci., 533 (2017) 141-159. https://doi.org/10.1016/j.memsci.2017.03.034

[32] J.F. Jhong, A. Venault, C.C. Hou, S.H. Chen, T.C. Wei, J. Zheng, J. Huang, Y. Chang, Surface zwitterionization of expanded poly(tetrafluoroethylene) membranes via atmospheric plasma-induced polymerization for enhanced skin wound healing, ACS Appl. Mater. Interfaces, 5 (2013) 6732-6742. https://doi.org/10.1021/am401669q

[33] Q. Li, Q.Y. Bi, B. Zhou, X.L. Wang, Zwitterionic sulfobetaine-grafted poly(vinylidene fluoride) membrane surface with stably anti-protein-fouling performance via a two-step surface polymerization, Appl. Surf. Sci., 258 (2012) 4707-4717. https://doi.org/10.1016/j.apsusc.2012.01.064

[34] Q. Li, B. Zhou, Q.Y. Bi, X.L. Wang, Surface modification of PVDF membranes with sulfobetaine polymers for a stably anti-protein-fouling performance, J. Appl. Polym. Sci., 125 (2012) 4015-4027. https://doi.org/10.1002/app.36715

[35] A. Zirehpour, A. Rahimpour, A. Arabi Shamsabadi, M. Sharifian Gh, M. Soroush, Mitigation of Thin-Film Composite Membrane Biofouling via Immobilizing Nano-Sized Biocidal Reservoirs in the Membrane Active Layer, Environ. Sci. Technol., 51 (2017) 5511-5522. https://doi.org/10.1021/acs.est.7b00782

[36] M. Yi, C.H. Lau, S. Xiong, W.J. Wei, R.Z. Liao, L. Shen, A. Lu, Y. Wang, Zwitterion-Ag complexes that simultaneously enhance biofouling resistance and silver binding capability of thin Zwitterion, ACS Appl. Mater. Interfaces, 11 (2019) 15698-15708. https://doi.org/10.1021/acsami.9b02983

[37] J. Wang, Z. Wang, Y. Liu, J. Wang, S. Wang, Surface modification of NF membrane with zwitterionic polymer to improve anti-biofouling property, 514 (2016) 407-417. https://doi.org/10.1016/j.memsci.2016.05.014

[38] D.Y. Zhang, Q. Hao, J. Liu, Y.S. Shi, J. Zhu, L. Su, Y. Wang, Antifouling polyimide membrane with grafted silver nanoparticles and zwitterion, 192 (2018) 230-239. https://doi.org/10.1016/j.seppur.2017.10.018

[39] A. Tiraferri, N.Y. Yip, A.P. Straub, S. Romero-Vargas Castrillon, M. Elimelech, A method for the simultaneous determination of transport and structural parameters of forward osmosis membranes, J. Membr. Sci., 444 (2013) 523-538. https://doi.org/10.1016/J.MEMSCI.2013.05.023

[40] M. Herzberg, S. Kang, M. Elimelech, Role of Extracellular Polymeric Substances (EPS) in Biofouling of Reverse Osmosis Membranes, Environ. Sci. Technol., 43 (2009) 4393-4398. https://doi.org/10.1021/es900087j

[41] Y. Pan, L.J. Ma, S. Lin, Y.F. Zhang, B.W. Cheng, J.Q. Meng, One-step bimodel grafting via a multicomponent reaction toward antifouling and antibacterial TFC RO membranes, J. Mater. Chem. A, 4 (2016) 15945-15960. https://doi.org/10.1039/c6ta05746b

[42] H.Y. Yu, Y. Kang, Y.L. Liu, B.X. Mi, Grafting polyzwitterions onto polyamide by click chemistry and nucleophilic substitution on nitrogen: A novel approach to enhance membrane fouling resistance, J. Membr. Sci., 449 (2014) 50-57. https://doi.org/10.1016/j.memsci.2013.08.022

[43] A.C. Fonseca, R.S. Summers, A.R. Greenberg, M.T. Hernandez, Extra-cellular polysaccharides, soluble microbial products, and natural organic matter impact on nanofiltration membranes flux decline, Environ. Sci. Technol., 41 (2007) 2491-2497. https://doi.org/10.1021/es060792i

[44] L.D. Nghiem, S. Hawkes, Effects of membrane fouling on the nanofiltration of trace organic contaminants, Desalination, 236 (2009) 273-281. https://doi.org/10.1016/j.desal.2007.10.077

[45] C. Boo, M. Elimelech, S. Hong, Fouling control in a forward osmosis process integrating seawater desalination and wastewater reclamation, J. Membr. Sci., 444 (2013) 148-156. https://doi.org/10.1016/j.memsci.2013.05.004

[46] H.Z. Shafi, Z. Khan, R. Yang, K.K. Gleason, Surface modification of reverse osmosis membranes with zwitterionic coating for improved resistance to fouling, Desalination, 362 (2015) 93-103. https://doi.org/10.1016/j.desal.2015.02.009

[47] M. Mozafari, S.F. Seyedpour, S.K. Salestan, A. Rahimpour, A.A. Shamsabadi, M.D. Firouzjaei, M.R. Esfahani, A. Tiraferri, H. Mohsenian, M. Sangermano, M. Soroush, Facile Cu-BTC surface modification of thin chitosan film coated polyethersulfone membranes with improved antifouling properties for sustainable removal of manganese, J. Membr. Sci., 588 (2019), 117200. https://doi.org/10.1016/j.memsci.2019.117200

[48] C.Y. Tang, Y.N. Kwon, J.O. Leckie, Effect of membrane chemistry and coating layer on physiochemical properties of thin film composite polyamide RO and NF membranes. I. FTIR and XPS characterization of polyamide and coating layer chemistry, Desalination, 242 (2009) 149-167. https://doi.org/10.1016/j.desal.2008.04.003

[49] D.I. Ellis, H. Muhamadali, M. Chisanga, R. Goodacre, Surface-Enhanced Raman Scattering (SERS) in Microbiology: Illumination and Enhancement of the Microbial World, Appl. Spectrosc., 72 (2018) 987-1000. https://doi.org/10.1177/0003702818764672

[50] D. Lin-Vien, N.B. Colthup, W.G. Fateley, J.G. Grasselli, The Handbook of Infrared and Raman Characteristic Frequencies of Organic Molecules, Academic Press, 1991.

[51] Y. Fan, C.J. Cornelius, Raman spectroscopic and gas transport study of a pentablock ionomer complexed with metal ions and its relationship to physical properties, J. Mater. Sci., 48 (2013) 1153-1161. https://doi.org/10.1007/s10853-012-6853-9

[52] A. Kaldor, A.G. Maki, A.J. Dorney, I.M. Mills, The assignment of v2 and v4 of SO3, J. Mol. Spectrosc., 45 (1973) 247-252. https://doi.org/10.1016/0022-2852(73)90155-0

[53] L. Rieppo, J. Töyräs, S. Saarakkala, Vibrational spectroscopy of articular cartilage, Appl. Spectrosc. Rev., 52 (2017) 249-266. https://doi.org/10.1080/05704928.2016.1226182

[54] N. Sundaraganesan, S. Ilakiamani, H. Saleem, P.M. Wojciechowski, D. Michalska, FT-Raman and FT-IR

spectra, vibrational assignments and density functional studies of 5-bromo-2-nitropyridine, Spectrochim. Acta, Part A, 61 (2005) 2995-3001. https://doi.org/10.1016/j.saa.2004.11.016

[55] A. Mekki, D. Holland, C.F. McConville, M. Salim, An XPS study of iron sodium silicate glass surfaces, 208 (1996) 267-276. https://doi.org/10.1016/S0022-3093(96)00523-6

[56] R. Precht, S. Stolz, E. Mankel, T. Mayer, W. Jaegermann, R. Hausbrand, Investigation of sodium insertion into tetracyanoquinodimethane (TCNQ): Results for a TCNQ thin film obtained by a surface science approach, 18 (2016) 3056-3064. https://doi.org/10.1039/c5cp06659j

[57] A.P. Savintsev, Y.O. Gavasheli, Z.K. Kalazhokov, K.K. Kalazhokov, X-ray photoelectron spectroscopy studies of the sodium chloride surface after laser exposure, in: Journal of Physics: Conference Series, 2016.

[58] Q.H. Wu, A. Thißen, W. Jaegermann, XPS and UPS study of Na deposition on thin film V 2 O 5, 252 (2005) 1801-1805. https://doi.org/10.1016/j.apsusc.2005.03.134

[59] R. Liu, Z. Xian, S. Zhang, C. Chen, Z. Yang, H. Li, W. Zheng, G. Zhang, H. Cao, Electrochemical-reduction-assisted assembly of ternary Ag nanoparticles/polyoxometalate/graphene nanohybrids and their activity in the electrocatalysis of oxygen reduction, RSC Adv., 5 (2015) 74447-74456. https://doi.org/10.1039/c5ra12556a

[60] J.A. Melero, R. van Grieken, G. Morales, M. Paniagua, Acidic mesoporous silica for the acetylation of glycerol: Synthesis of bioadditives to petrol fuel, Energy Fuels, 21 (2007) 1782-1791. https://doi.org/10.1021/ef060647q

[61] G. Beamson, D. Briggs, High Resolution XPS of Organic Polymers: The Scienta ESCA300 Database, 70 (1993), A25. https://doi.org/10.1021/ed070pa25.5

[62] K. Fatyeyeva, J. Bigarré, B. Blondel, H. Galiano, D. Gaud, M. Lecardeur, F. Poncin-Epaillard, Grafting of p-styrene sulfonate and 1,3-propane sultone onto Laponite for proton exchange membrane fuel cell application, J. Membr. Sci., 366 (2011) 33-42. https://doi.org/10.1016/j.memsci.2010.09.023

[63] A. Mohtasebi, T. Chowdhury, L.H.H. Hsu, M.C. Biesinger, P. Kruse, Interfacial Charge Transfer between Phenyl-Capped Aniline Tetramer Films and Iron Oxide Surfaces, J. Phys. Chem. C, 120 (2016) 29248-29263. https://doi.org/10.1021/acs.jpcc.6b09950

[64] S. Yuan, G. Xiong, A. Roguin, S. Hin, C. Choong, Amelioration of Blood Compatibility and Endothelialization of Polycaprolactone Substrates by Surface-Initiated Atom Transfer Radical Polymerization, in: Advances in Biomaterials Science and Biomedical Applications, InTech, 2013.

[65] M.D. Firouzjaei, A.A. Shamsabadi, S.A. Aktij, S.F. Seyedpour, M. Sharifian Gh, A. Rahimpour, M.R. Esfahani, M. Ulbricht, M. Soroush, Exploiting Synergetic Effects of Graphene Oxide and a Silver-Based Metal–Organic Framework To Enhance Antifouling and Anti-Biofouling Properties of Thin-Film Nanocomposite Membranes, ACS Appl. Mater. Interfaces, 10 (2018) 42967-42978. https://doi.org/10.1021/acsami.8b12714

[66] X. Gu, S. Bi, L. Guo, Y. Zhao, T. Li, M. Liu, P. Chen, Y. Wu, Facile Fabrication of Ordered Component-Tunable Heterobimetallic Self-Assembly Nanosheet for Catalyzing "click" Reaction, ACS Omega, 2 (2017) 5415-5433. https://doi.org/10.1021/acsomega.7b00364

[67] J. Li, Y. Xie, Y. Zhong, Y. Hu, Facile synthesis of Z-scheme Ag2CO3/Ag/AgBr ternary heterostructured nanorods with improved photostability and photoactivity, J. Mater. Chem. A, 3 (2015) 5474-5481. https://doi.org/10.1039/c4ta06075j

[68] W. Song, B. Hong, S. Hong, Y. Lai, J. Li, Y. Liu, Effect of prop-1-ene-1,3-sultone on the performances of

lithium cobalt oxide/graphite battery operating over a wide temperature range, Int. J. Electrochem. Sci., 12 (2017) 10749-10762. https://doi.org/10.20964/2017.11.84

[69] W. Yao, Z. Zhang, J. Gao, J. Li, J. Xu, Z. Wang, Y. Yang, Vinyl ethylene sulfite as a new additive in propylene carbonate-based electrolyte for lithium ion batteries, Energy Environ. Sci., 2 (2009) 1102-1108. https://doi.org/10.1039/b905162g

[70] H. Guo, Y. Zhang, Z. Zheng, H. Lin, Y. Zhang, Facile one-pot fabrication of Ag@MOF(Ag) nanocomposites for highly selective detection of 2,4,6-trinitrophenol in aqueous phase, Talanta, 170 (2017) 146-151. https://doi.org/10.1016/j.talanta.2017.03.096

[71] R. Liu, X. Yu, G. Zhang, S. Zhang, H. Cao, A. Dolbecq, P. Mialane, B. Keita, L. Zhi, Polyoxometalate-mediated green synthesis of a 2D silver nanonet/graphene nanohybrid as a synergistic catalyst for the oxygen reduction reaction, J. Mater. Chem. A, 1 (2013) 11961-11969. https://doi.org/10.1039/c3ta12941a

[72] E.M. Vrijenhoek, S. Hong, M. Elimelech, Influence of membrane surface properties on initial rate of colloidal fouling of reverse osmosis and nanofiltration membranes, J. Membr. Sci., 188 (2001) 115-128. https://doi.org/10.1016/S0376-7388(01)00376-3

[73] X. Lu, S. Romero-Vargas, C.n. Castrillón, D.L. Shaffer, J. Ma, M. Elimelech, In Situ Surface Chemical Modification of Thin-Film Composite Forward Osmosis Membranes for Enhanced Organic Fouling Resistance, Environ. Sci. Technol., 47 (2013) 12219-12228. https://doi.org/10.1021/es403179m

[74] B.X. Mi, M. Elimelech, Organic fouling of forward osmosis membranes: Fouling reversibility and cleaning without chemical reagents, J. Membr. Sci., 348 (2010) 337-345. https://doi.org/10.1016/j.memsci.2009.11.021

[75] A. Tiraferri, C.D. Vecitis, M. Elimelech, Covalent Binding of Single-Walled Carbon Nanotubes to Polyamide Membranes for Antimicrobial Surface Properties, ACS Appl. Mater. Interfaces, 3 (2011) 2869-2877. https://doi.org/10.1021/am200536p

[76] K. Seo, M. Kim, D.H. Kim, Re-derivation of Young's Equation, Wenzel Equation, and Cassie-Baxter Equation Based on Energy Minimization, in: M. Aliofkhazraei (Ed.) Surface Energy, 2016, pp. 1-21.

[77] A. Soroush, W. Ma, Y. Silvino, M.S. Rahaman, Surface modification of thin film composite forward osmosis membrane by silver-decorated graphene-oxide nanosheets, Environ. Sci.: Nano, 2 (2015) 395-405. https://doi.org/10.1039/c5en00086f

[78] N.T. Hancock, T.Y. Cath, Solute Coupled Diffusion in Osmotically Driven Membrane Processes, Environ. Sci. Technol., 43 (2009) 6769-6775. https://doi.org/10.1021/es901132x

[79] W.A. Phillip, J.S. Yong, M. Elimelech, Reverse Draw Solute Permeation in Forward Osmosis: Modeling and Experiments, Environ. Sci. Technol., 44 (2010) 5170-5176. https://doi.org/10.1021/es100901n

[80] Q. She, X. Jin, C.Y. Tang, Osmotic power production from salinity gradient resource by pressure retarded osmosis: Effects of operating conditions and reverse solute diffusion, J. Membr. Sci., 401-402 (2012) 262-273. https://doi.org/10.1016/J.MEMSCI.2012.02.014

[81] D.L. Shaffer, J.R. Werber, H. Jaramillo, S.H. Lin, M. Elimelech, Forward osmosis: Where are we now?, Desalination, 356 (2015) 271-284. https://doi.org/10.1016/j.desa12014.10.031

[82] S.F. Seyedpour, A. Rahimpour, G. Najafpour, Facile in-situ assembly of silver-based MOFs to surface functionalization of TFC membrane: A novel approach toward long-lasting biofouling mitigation, J. Membr. Sci., 573 (2019) 257-269. https://doi.org/10.1016/j.memsci.2018.12.016

[83] G. Wyszogrodzka, B. Marszałek, B. Gil, P. Dorozyński, Metal-organic frameworks: Mechanisms of antibacterial action and potential applications, Drug Discovery Today, 21 (2016) 1009-1018. https://doi.org/10.1016/j.drudis.2016.04.009

[84] J. Wu, W. Lin, Z. Wang, S. Chen, Y. Chang, Investigation of the Hydration of Nonfouling Material Poly(sulfobetaine methacrylate) by Low-Field Nuclear Magnetic Resonance, Langmuir, 28 (2012) 7436-7441. https://doi.org/10.1021/la300394c

[85] L. Shen, X. Zhang, J. Zuo, Y. Wang, Performance enhancement of TFC FO membranes with polyethyleneimine modification and post-treatment, J. Membr. Sci., 534 (2017) 46-58. https://doi.org/10.1016/J.MEMSCI.2017.04.008